JOURNAL OF GEOPHYSICAL RESEARCH, VOL. 100, NO. B2, PAGES 2261–2278, FEBRUARY 10, 1995

Extinct spreading center in the Labrador Sea: Crustal structure from a two-dimensional seismic refraction velocity model

John C. Osler[1] and Keith E. Louden

Department of Oceanography, Dalhousie University, Halifax, Nova Scotia, Canada

Abstract. The Labrador Sea contains a rare example of an abandoned mid-ocean ridge where active accretion of oceanic crust ceased due to a change in the spreading geometry of lithospheric plates. Seismic refraction data were collected along a line which transversely crosses the extinct spreading center. Two-dimensional analyses of the refraction data, using ray-tracing and synthetic seismogram techniques reveal major variations in crustal thickness and velocity in relation to the axis of the extinct spreading center. In the extinct spreading center, a crustal thickness of approximately 4 km is determined, compared with 5.5 km for the flanks. Substantial lateral variations in *P* wave velocities of the upper and lower crust are observed with a marked decrease within the extinct spreading center. Low velocities are also observed in the uppermost mantle underlying the extinct spreading center and are interpreted as being the result of hydrothermal alteration. The anomalously low crustal velocities and crustal thinning are attributed to a decreasing supply of partial melt and increasing degree of tectonism at the slow spreading rates preceding extinction.

Introduction

Mid-ocean ridges mark the boundaries between diverging lithospheric plates where new oceanic crust and lithosphere are formed. Extinct spreading centers are mid-ocean ridges where the active accretion of oceanic crust has ceased due to a change in the spreading geometry of the lithospheric plates. They are large-scale features formed by ridge jumps in excess of 400 km between the extinct spreading center and the new locus of rifting [*Batiza*, 1989]. They can be identified by their morphological expression [*Mammerickx and Sandwell*, 1986] and magnetic anomaly pattern. Extinct spreading centers identified on this basis are the Mathematician Ridge [*Klitgord and Mammerickx*, 1982]; the Galapagos Ridge [*Anderson and Sclater*, 1972]; the Aegir Ridge [*Talwani and Eldholm*, 1977]; the Central Basin Fault [*Lewis and Hayes*, 1980]; the Shikoku Ridge [*Tomoda et al.*, 1975]; and ridges in the Tasman [*Weissel and Hays*, 1977], Coral [*Weissel and Watts*, 1979] and Labrador Seas [*Srivastava et al.*, 1981]. Few refraction studies have been conducted at these extinct spreading centers. *Nagumo et al.* [1980] published refraction profiles sampling the upper crust in the vicinity of the Shikoku Ridge in the Philippine Sea, and seismic refraction lines have been shot across the Aegir Ridge in the Norwegian-Greenland Sea, but this material remains unpublished (R. B. Whitmarsh, personal communication, 1992).

This paper presents a two-dimensional analysis of seismic refraction data collected on a line which traverses the extinct spreading center in the Labrador Sea. The two-dimensional (2-D) velocity-depth structure, developed by ray-tracing and synthetic seismogram techniques, shows the crust within the extinct spreading center to be thin and of anomalously low *P* wave velocity relative to its flanks. Likewise, low velocities are observed in the uppermost mantle, underlying the crust within the extinct spreading center. Two potential mechanisms for forming these crust and upper mantle structures are explored. The preferred interpretation is that decreases in spreading rate led to an enhanced conductive cooling of the crust rendering it brittle and subject to tectonism. The tectonism produces low crustal velocities by fracturing the crust and may cause some crustal thinning through the rotation of crustal blocks on major faults. The tectonism promotes deep penetration of hydrothermal fluids reducing partial melt supply which yields thinner crust. The hydrothermal circulation penetrates through the crust allowing serpentinization of the upper mantle thereby reducing its velocity.

The anomalous crust at the extinct spreading center formed in the time interval from Chron 21 until its extinction. Modeling of magnetic anomaly patterns [*Osler*, 1993] suggests that spreading did not cease instantaneously but was protracted over the period from Chron 21 to 13. The variation in the observed crustal structure in relation to the paleorift axis supports the idea of a systematic relationship between slow spreading rates and (1) increased tectonism; (2) decreased partial melt supply; (3) hydrothermal alteration of the uppermost mantle; and (4) crustal thickness.

Geological Setting

The Labrador Sea is a small ocean basin confined between the coasts of Labrador and Baffin Island to the west and Greenland to the east (Figure 1). The presence of a buried extinct ridge in the Labrador Sea was first suggested by *Drake et al.* [1963] based on seismic reflection profiles, although at that time the oceanic affinity of the crust in the basin was unclear [*Van der Linden*, 1975]. From detailed analysis of the

[1]Now at Defence Research Establishment Atlantic, Darmouth, Nova Scotia, Canada.

Paper number 94JB02890.
0148-0227/95/94JB-02890$05.00

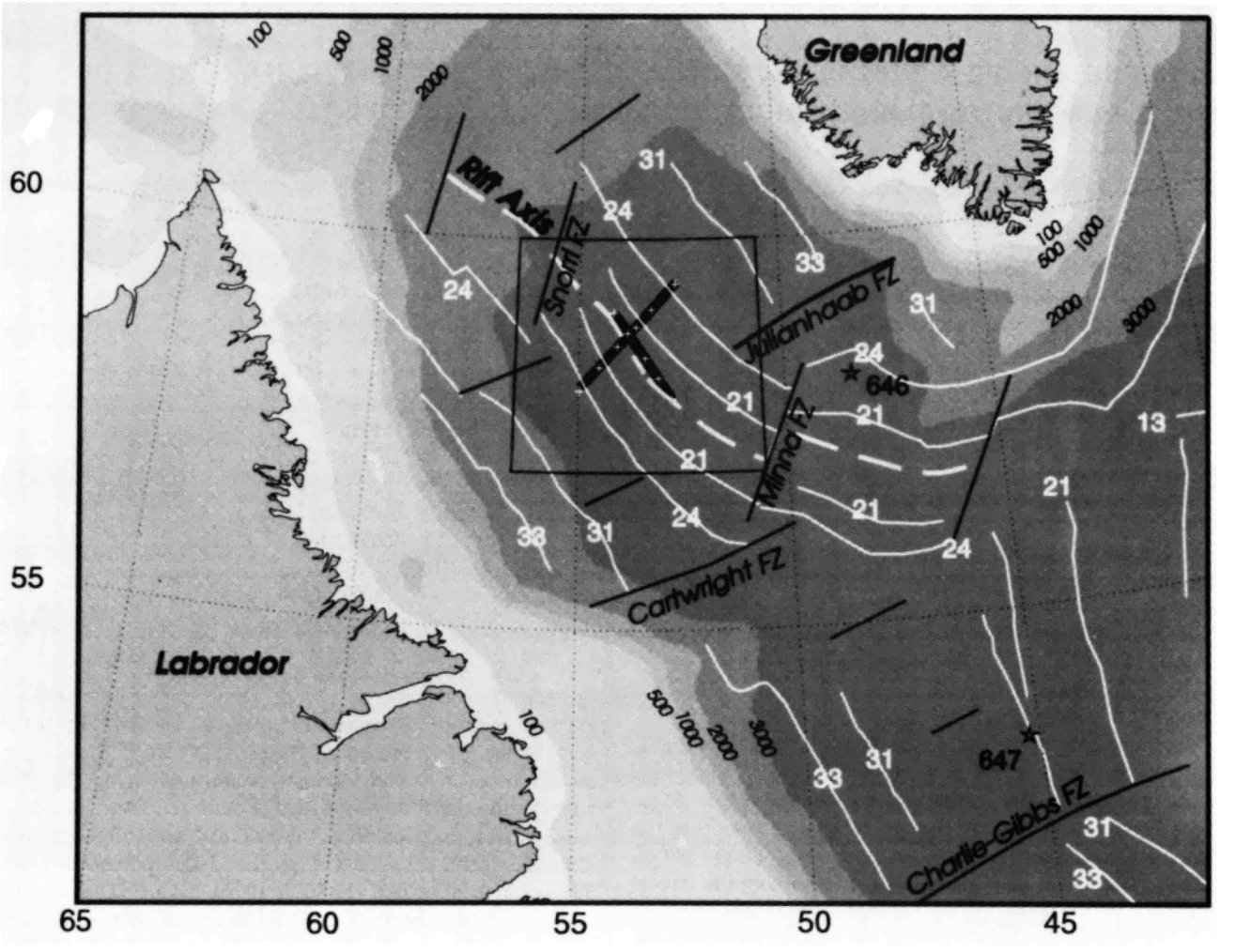

Figure 1. Location map for the seismic refraction experiment in the Labrador Sea. The thick solid lines are refraction profiles; open crosses are locations of ocean bottom seismometer (OBS) receivers. Thinner solid lines are fracture zones [*Roest and Srivastava*, 1989b]. Selected bathymetry contour levels (as indicated in meters) are shaded in grey. Selected magnetic anomaly lineations and corresponding Chronological identifiers are from *Srivastava et al.* [1988]. Ocean Drilling Program (ODP) Sites 646 and 647 are indicated by stars.

magnetic anomalies in the basin, its seafloor spreading history has been most recently documented by *Roest and Srivastava* [1989a], as follows. After a period of continental stretching, spreading was initiated south of the Cartwright Fracture Zone at Chron 34 (84 Ma, following the timescale of *Kent and Gradstein* [1986]) and was established in the northern Labrador Sea, south of Davis Strait, by Chron 31 (69 Ma). Spreading continued in an east-northeast direction until Chron 25 (59 Ma) when a major reorientation of spreading occurred. The reorientation to a more oblique spreading direction (north-northeast) was coincident with the onset of hot spot activity in Davis Strait [*Hyndman*, 1973; *Srivastava et al.*, 1989] and the separation of Greenland from Eurasia. A triple junction south of Greenland existed during simultaneous seafloor spreading between North America and Greenland and Greenland and Eurasia, between Chron 24 (56 Ma) and Chron 20 (45 Ma)

Spreading continued in the Labrador Sea until Chron 20 (45 Ma, Figure 2) and was abandoned sometime before Chron 13 (36 Ma) which is the first anomaly in the North Atlantic parallel to and continuous with the present Mid-Atlantic Ridge [*Kristoffersen and Talwani*, 1977]. Spreading rate histories are provided by *Roest and Srivastava* [1989a] for a section of the extinct spreading center northwest of the Snorri fracture zone (Figure 1) and by *Osler* [1993] for the segment of the extinct spreading center under consideration in this study. *Roest and Srivastava* [1989a] propose half spreading rates of 18.2, 9.4, and 2.7 mm/yr for Chrons 25 to 24, 24 to 21 and 21 to 13, respectively. *Osler* [1993] proposes half spreading rates of 6.9 and 7.0 mm/yr for Chrons 25 to 24 and 24 to 21, respectively, followed by a linear decrease in spreading rate as a function of time from 5.01 to 0 mm/yr between Chrons 21 and 13. The modeling of spreading rate histories is hampered by the low amplitude of the magnetic anomalies from Chron 24 to the extinct spreading center. They may be muted due to the probability of rocks with mixed geomagnetic polarities occurring in a vertical column at slow spreading rates [*Denham and Schouten*, 1979] or greater segmentation of the ridge axis during oblique spreading juxtaposing crustal blocks of normal and reversed polarity across many small offset transform faults [*Roots and Srivastava*, 1984].

Experimental Procedure

Two long refraction lines were shot at the extinct spreading center in the Labrador Sea (Figure 2) in 1987. Line R1, 150 km in length, was situated to sample crust along its strike, and line R2, 220 km in length, crossed it transversely to sample crust away from the area of the extinct spreading center out to Chron 24 in order to measure variations in crustal thickness as the extinct spreading center is approached. R2 was oriented parallel to the general direction of spreading following the major reorientation at magnetic anomaly 25 [*Srivastava*, 1978]. A reexamination of the magnetic anomalies [*Roest and Srivastava*, 1989a], following the collection of the refraction data, altered the strike of this flow line by approximately 20° to the north. Hence line R2 does not exactly follow a flow line.

The refraction lines were positioned to avoid the known fractures zones in the area (Figure 1): the Snorri Fracture Zone to the northwest and the Minna and Julianhaab fracture zones to the southeast [*Srivastava et al.*, 1988]. The determination of fracture zone locations in the Labrador Sea is guided chiefly by their signature in the free-air gravity field, where they

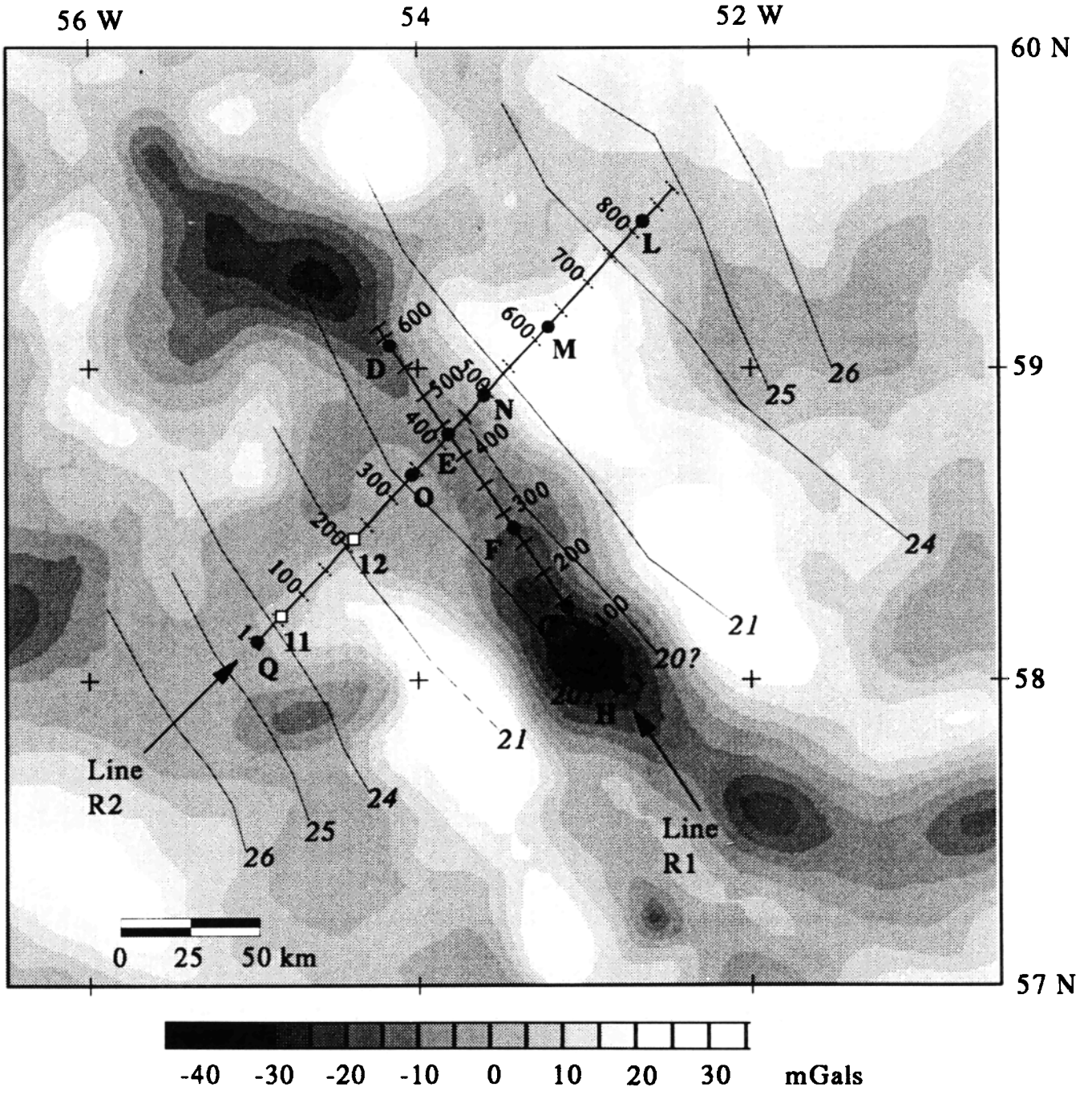

Figure 2. Shot point and receiver locations (OBSs, solid lettered circles, and sonobuoys, open numbered squares) for the seismic refraction experiment. The axis of the extinct spreading center is along the prominent low in the free-air gravity anomaly [from *Woodside*, 1989]. Magnetic lineations and chronological identifiers follow the interpretation of *Roest and Srivastava* [1989a].

appear as prominent, low-amplitude lineations. In positioning the refraction lines, these prominent features in the free-air gravity anomaly field were avoided. The possibility that fracture zone features are influencing the seismically determined crustal structures along the refraction lines is thus considered minimal but cannot be excluded.

Free fall/pop-up ocean bottom seismometers (OBSs) [*Loncarevic*, 1983] from Dalhousie University and the Atlantic Geoscience Center (Bedford Institute of Oceanography) were deployed at locations (Figure 2) along lines R1 (five OBSs) and R2 (eight OBSs). The spacing between OBSs was approximately 20 km at the extinct spreading center and up to 50 km on the flanks. In the following sections, each seismic record is referred to by the OBS letter and the direction of shooting (e.g., OBS M_{SW}). An array of 6 x 16.4 L (6 x 1000 in^3) air guns was used as the seismic source with a trace separation of approximately 250 m (shot point locations in Figure 2). Single-channel reflection data were collected simultaneously. Disposable sonobuoys were deployed between OBS positions (Figure 2) and recorded on analog FM tape. Two of these, S/B 11 and 12, were used in the subsequent analysis because of a failure of one OBS.

For each OBS, timing corrections are applied to account for (1) offsets and drifts in the OBS clock and (2) offsets between analog data channels due to tape head misalignment. The first correction could leave a travel time error of no more than 12 ms, which is equivalent to one sample point and is not significant. The second correction is treated as having a static component, which is determined every 24 hours by applying a calibration tone to all channels, and a dynamic component that arises from irregular tape transport. The offset due to this component may be up to 1/4 of a seismic period between successive shots, but its effect is removed by trace mixing. Shot point locations were obtained using a combination of Loran C and transit satellite fixes, smoothed by a running mean applied along a 6-min window. Instrument locations were determined by creating a reference grid and then searching this grid to find the location where there is a least squares minimum between ranges from water wave arrival times, ray traced through a water velocity structure to their respective shot points, and ranges from a position on the reference grid to the shot points. A detailed discussion and listing of uncertainties in OBS and shot point positions is given by *Osler* [1993].

Two-Dimensional Velocity Structure of Line R2 From Travel Time Modeling

Model Parameterization

The RAYINVR package of *Zelt and Smith* [1992] was used in developing a 2-D seismic crustal structure. Computed arrival times for user selected refracted, head wave or reflected phases are determined by raytracing through an irregular network of layered trapezoidal blocks which are used to parameterize the velocity structure. The ray tracing through the velocity model is performed using zero-order asymptotic ray theory [*Cerveny et al.*, 1977]. Criteria which guide the specification of nodes for each layer are (1) ray coverage; (2) auxiliary data sources (e.g., 12 kHz bathymetry and single channel seismic reflection data); and (3) trade-offs between RMS travel time residuals, T_{RMS}, and resolution. The number and distribution of nodes along line R2 are shown in Figure 3.

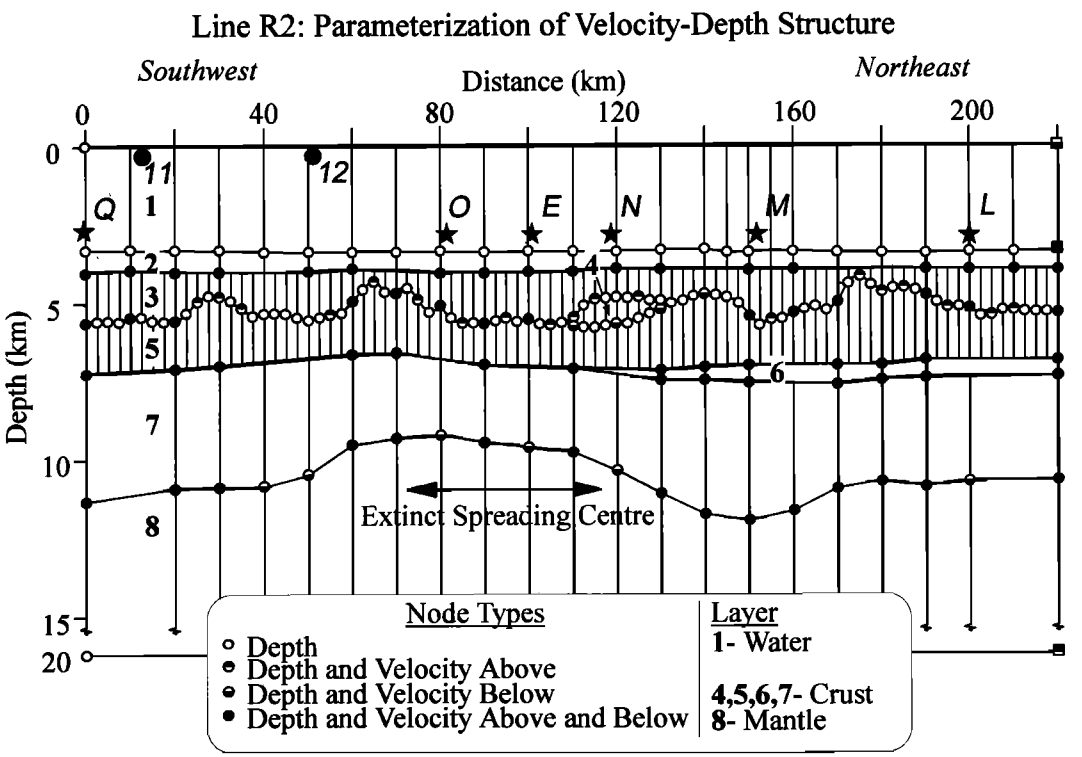

Figure 3. The 2-D model of the velocity-depth structure along refraction line R2 is parameterized by a series of layered trapezoidal blocks. Each layer is defined by a series of boundary nodes along its upper surface and velocity nodes along its upper and lower surfaces (values for each node are listed in Table 2, electronic supplement). OBS and sonobuoy positions are indicated by stars and circles, respectively.

Employing these criteria results in a basic along track nodal spacing of 10 km, although there are several areas along the refraction line with a differing nodal density. A first example is the sediment-crust boundary (between layers 3 and 4 or 3 and 5 in Figure 3) where nodes are specified every 2.5 km as required by observed travel time variations (e.g., oscillation of the observed travel time of P_n arrivals for OBS M_{SW} between 60 and 80 km in Figure 9a). Another example is the absence of boundary and velocity nodes in the crust between 30 and 60 km (layers 5 and 7 in Figure 3), where the paucity of raypaths traveling through this region precludes the specification of nodes. A third example is the lower crust within the extinct spreading center from 70 to 90 km (Figure 3), where lateral velocity variations are moderate and do not require a smaller nodal spacing.

Initial Velocity-Depth Model

The water column is treated as a single layer with a uniform velocity of 1.49 km/s. Bottom boundary nodes were determined from the 12-kHz bathymetry and specified every 2.5 km. The sediment column is divided into two layers. The first layer is between the seafloor and an internal sediment reflector at an average two way travel time of 0.68 s below the seafloor, marking the transition from the reflective upper section to the transparent lower section (Figure 4). This reflector correlates with reflector R1 identified on other reflection profiles in the Labrador Sea [*Srivastava et al.*, 1989] and corresponds to the bottommost occurrence of ice-rafted debris at Ocean Drilling Program (ODP) Site 646, dated as mid to late Pliocene. The second layer is defined between the internal sediment reflector and the sediment-crust boundary. For a linear increase in velocity as a function of depth, where k is the velocity gradient, z_{lower} is the layer thickness, and V_{upper} and V_{lower} are the velocities at the top and bottom of the layer respectively, the normal incidence travel time, ΔT, within a layer is

$$\Delta T = \frac{1}{k} ln\left(1+\frac{kz_{lower}}{V_{upper}}\right). \quad (1)$$

The layer depth and lower boundary velocity are

$$z_{lower} = \frac{\Delta T(V_{lower}-V_{upper})}{ln\left(1+\frac{V_{lower}-V_{upper}}{V_{upper}}\right)} \quad (2)$$

$$V_{lower} = V_{upper} + kz_{lower}. \quad (3)$$

For the upper sediment layer, the velocity log at ODP Site 646 [*Jarrard et al.*, 1989, Figure 16] is used to assign V_{upper}=1.5 km/s and k=0.96 s^{-1}. Using these values, the computed depth to the internal sediment reflector averages 0.63 km for refraction line R2, which coincides with the depth at which the velocity gradient decreases markedly in the Site 646 velocity log. For the lower sediment layer, the observed travel times from rays refracted within the layer are used to select values of V_{upper}=2.2 km/s and k=0.2 s^{-1}. The nodes computed with these values require little modification in the modeling, except in the area of the extinct spreading center, where V_{upper} and k both increase.

The specification of boundary and velocity nodes for the upper crust, lower crust, and mantle layer is based on 1-D travel time solutions. For each OBS, the τ-p velocity-depth structures [*Osler and Louden*, 1992] are divided into upper and

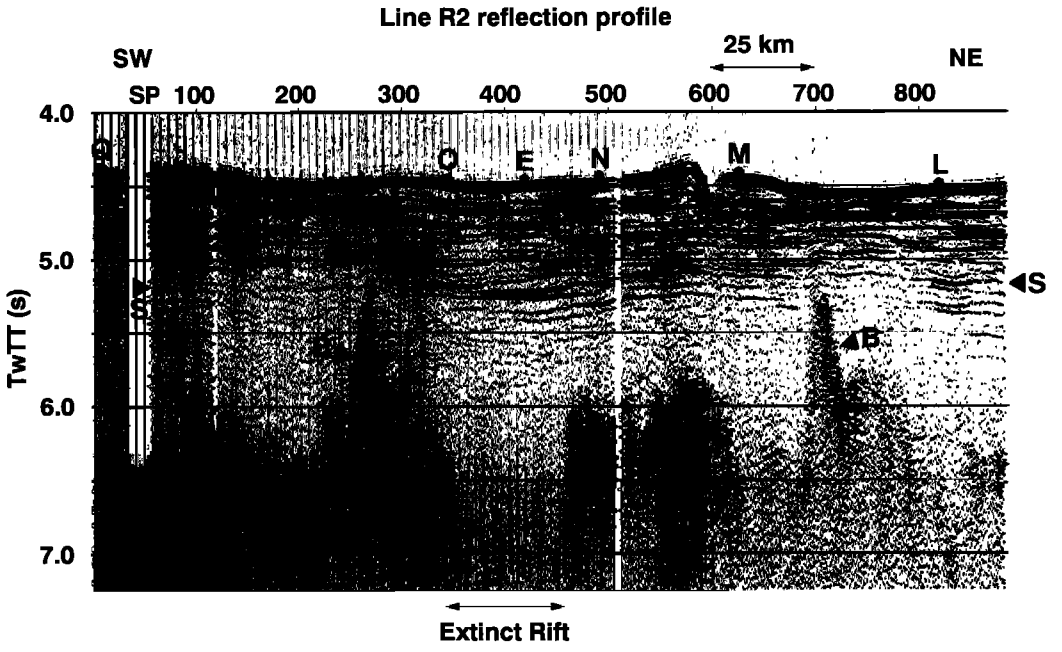

Figure 4. Single-channel reflection profile along line R2. Individual traces are band-pass filtered from 6 to 36 Hz, amplitude squared to increase signal to noise, and multiplied by a time-varying gain function to compensate for energy loss due to spreading. OBS locations are indicated by solid circles; pointers locate sediment-basement (B) and upper and lower sediment (S) interfaces. Vertical exaggeration is 30:1.

lower crustal layers at a depth where the velocity gradient may be split into two linear segments offset by a velocity discontinuity, if required. The layer thicknesses and velocities are used to define the structure of the crust at a point offset laterally from the receiver by 10 km in the direction of shooting. In cases where the lateral offset causes structures from adjacent receivers to overlap (e.g., OBS O_{NE} and OBS E_{SW}), the structures are averaged and placed at a distance midway between receivers.

Mantle velocities are taken from the slope-intercept velocity-depth structures [*Osler and Louden*, 1992]. The mantle velocity nodes are offset laterally from the receiver by 10 km in the direction of shooting. For defining the lower boundary of the mantle layer, a velocity of 8.24 km/s is specified at a depth of 20 km. This introduces vertical velocity gradients which range from 0.02 s-1 to 0.04 s-1 depending on the velocity at the upper boundary of the mantle layer. For most OBSs, this gradient provides a suitable match for the critical range beyond which mantle refracted phases begin to be observed. The irregular distribution of boundary and velocity nodes for the crustal and mantle layers is interpolated to form a regular grid with a nodal spacing of 10 km.

Model Revisions

An optimal fit between observed and computed travel times is sought by adjusting the initial velocity and boundary nodes. By assigning uncertainties to observed travel time picks, the quality of a computed travel time fit may be assessed numerically (equation (5) below). For all travel time picks, a base uncertainty of ± 0.02 s has been chosen to account for the timing uncertainties inherent in the refraction data. A further uncertainty has been added to reflect the quality of the pick itself. The largest uncertainties of ± 0.12 s have been assigned to P_mP and sediment refraction arrivals, which are difficult to pick because of interference from first arrivals, and to P_n arrivals, which are difficult to pick because of their low signal to noise.

To assess the quality of successive model iterations, three parameters were compared. First, one seeks a velocity-depth structure which maximizes the number of observed locations to which rays may be traced, n. The parameters T_{RMS} and χ^2 quantify the fit between the observed and computed arrival times for a given ray group and are defined as follows

$$T_{RMS} = \left(\frac{\sum_{i=1}^{n} (T_{obs_i} - T_{calc_i})^2}{n} \right)^{1/2} \quad (4)$$

$$\chi^2 = \left(\frac{\sum_{i=1}^{n} \left(\frac{T_{obs_i} - T_{calc_i}}{U_{obs_i}} \right)^2}{n} \right)^{1/2} \quad (5)$$

where T_{obs} is observed travel time, T_{calc} is calculated travel time, U_{obs} is uncertainty of the observed travel time, and n is number of calculated travel times reaching observed arrivals. For values of $\chi^2 \leq 1$, the computed arrivals fit the observed arrivals within the uncertainties of the observed travel times, providing an acceptable model revision. This minimum standard is only relaxed when multiple ray paths from different receivers overlap, but no structure can be devised which is capable of allowing $\chi^2 \leq 1$ for all receivers.

Final Model

In Figure 5, the final velocity-depth structure is represented by smoothed isovelocity contours, calculated every 1 km by a linear interpolation between the velocity and boundary nodes for the trapezoid in which they are bounded. Contours can become coincident along model boundaries where there is a velocity contrast (e.g., the sediment-crust boundary). Figures 6 and 7 present ray paths through the layers of the final velocity-depth structure and their associated observed and computed travel times. The values of n, T_{RMS}, and χ^2 in the final velocity-depth structure are presented in Table 1[1] (electronic supplement).

Sediment Layers. The sediment layers are numbered 2 and 3 in the model parameterization (Figure 3). Ray paths and associated travel times for sediment refractions are found in Figure 6a. Comparison of computed and observed arrivals for OBSs L, M, and Q_{NE} exemplify the excellent fit provided by the model (χ^2 values from 0.057 to 0.140). Maximum shot-receiver offsets for computed sediment refractions correspond closely to observations, indicating that the vertical velocity gradients have been appropriately specified. For sediments within the extinct rift valley (nodes from approximately 80 to 120 km), the velocity of nodes along the top and bottom of the lower sediment layer (layer 3) must be increased. The requirement for higher velocities is indicated in Figure 6a by OBS E and OBS O_{NE}, which have velocities exceeding 2.5 km/s, while receivers outside this region have velocities slower than 2.5 km/s. The topography of the sediment-crust boundary (interfaces 3 and 4 or 3 and 5 in Figure 3) has been modified to improve the travel time fit of the crustal and mantle arrivals in regions where the basement reflector is difficult to pick. Two notable examples are (1) the short-wavelength oscillations introduced on the basement high from 60 to 80 km to reproduce the travel time oscillations observed in P_n for OBS N_{SW}, OBS E_{SW}, and OBS M_{SW} and (2) the deepening of the sediment-crust boundary around 150 km to delay crustal arrivals.

Crustal Layers. The 2-D velocity-depth structure quantifies the lateral variations in the crust across the extinct spreading center. The model layers which define the crust are numbered 4, 5, 6, and 7 in the model parameterization (Figure 3). Ray paths and travel times are presented in Figure 6b for the upper crust and in Figure 6c for the lower crust. Two principal variations in crustal structure emerge: (1) the variation in the velocity and thickness of the crust across the

[1]An electronic supplement of Tables 1 and 2 may be obtained on a diskette or Anonymous FTP from KOSMOS.AGU.ORG. (LOGIN to AGU's FTP account using ANONYMOUS as the username and GUEST as the password. Go to the right directory by typing CD APEND. Type LS to see what files are available. Type GET and the name of the file to get it. Finally, type EXIT to leave the system.) (Paper 94JB02890, Extinct spreading center in the Labrador Sea: Crustal structure from a two-dimensional seismic refraction velocity model, by J. C. Osler and Keith E. Louden). Diskette may be ordered from American Geophysical Union, 2000 Florida Avenue, N.W., Washington, DC 20009; $15.00. Payment must accompany order.

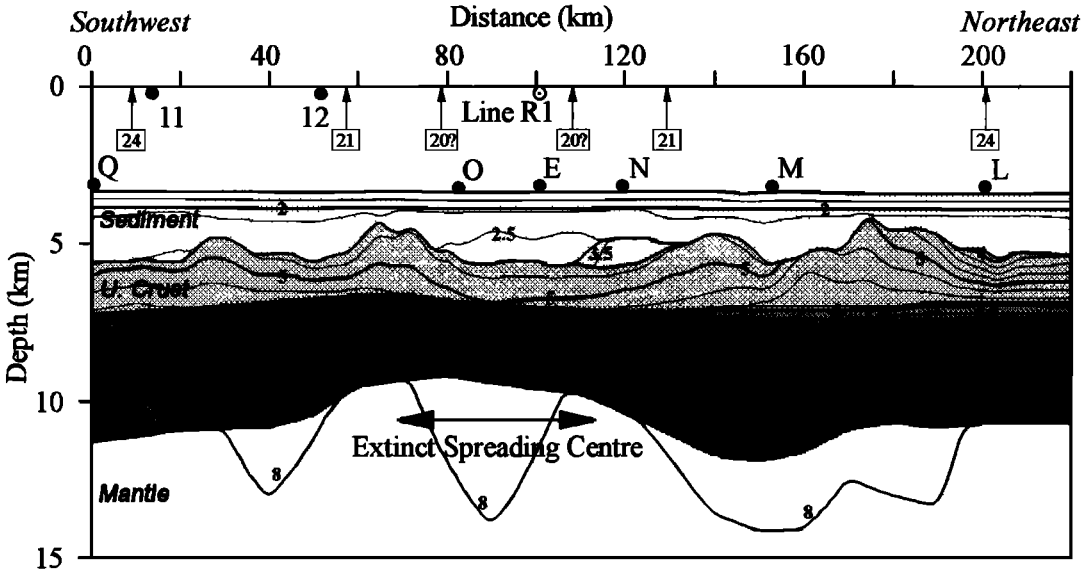

Figure 5. The 2-D velocity-depth structure is represented by isovelocity contours, drawn every 0.25 km/s, which can become coincident along model boundaries where a velocity discontinuity is present. Layers in the model parameterization (Figure 4) are distinguished by different grey tones. Receivers are denoted by solid circles. Arrows and corresponding chronological identifiers mark the intersection of magnetic anomaly lineations with line R2. Selected velocity contours are labeled in kilometers per second.

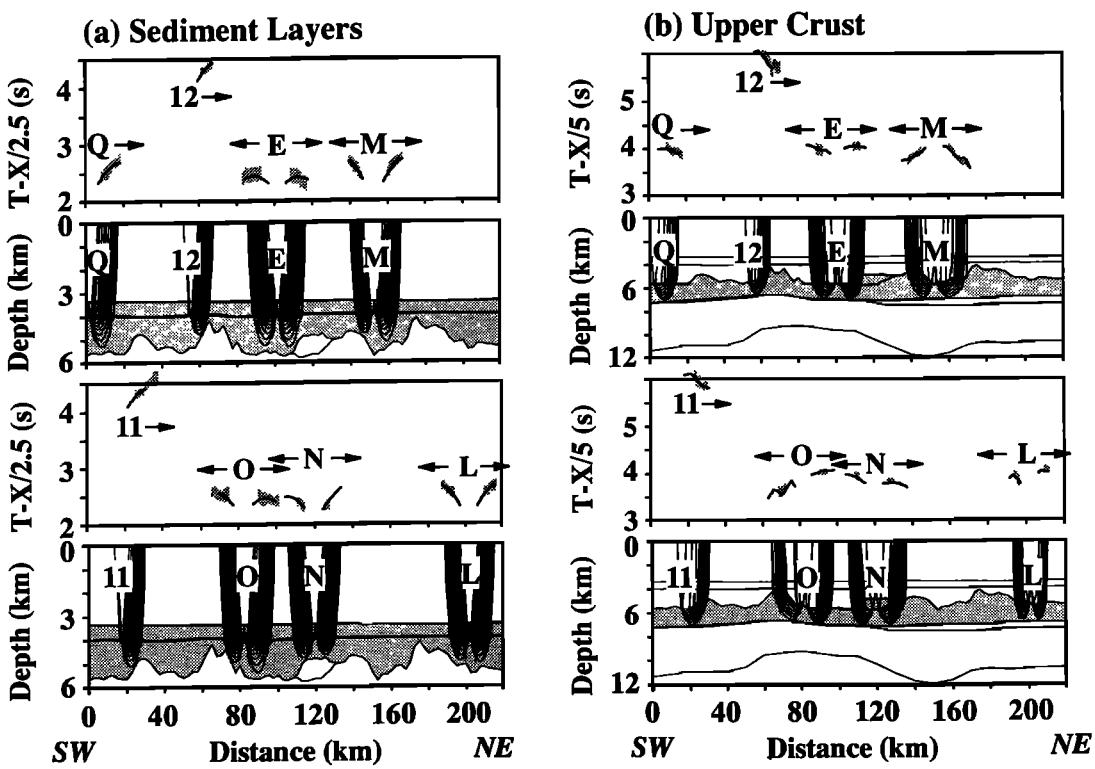

Figure 6. Computed ray paths and travel times using the 2-D velocity-depth structure along line R2 for (a) refractions in the sediment layer (b) refractions in the upper crust, P_2 (c) refractions in the lower crust, P_3, and (d) mantle wide-angle reflections, P_mP. Observed travel times and their uncertainties are represented by the stippled areas through which the computed arrival times are traced. Ray paths converge to their corresponding receivers. For clarity, the diagrams show every other OBS for each line so that arrival times can be discriminated.

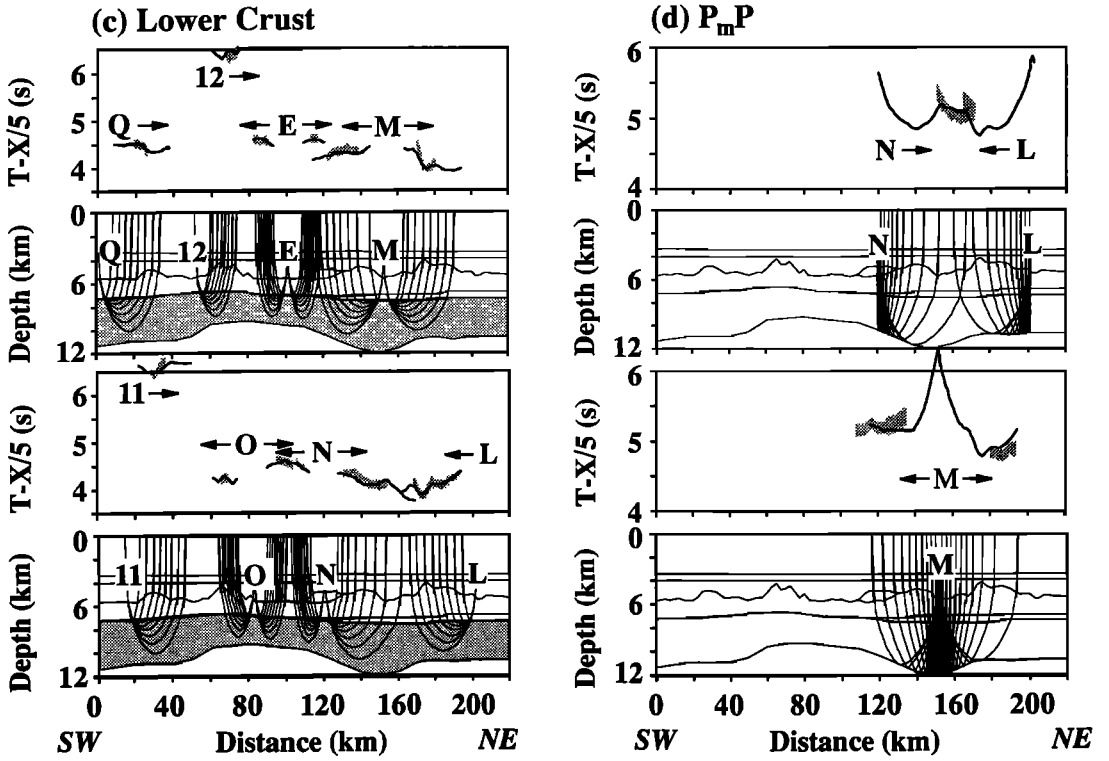

Figure 6. (continued)

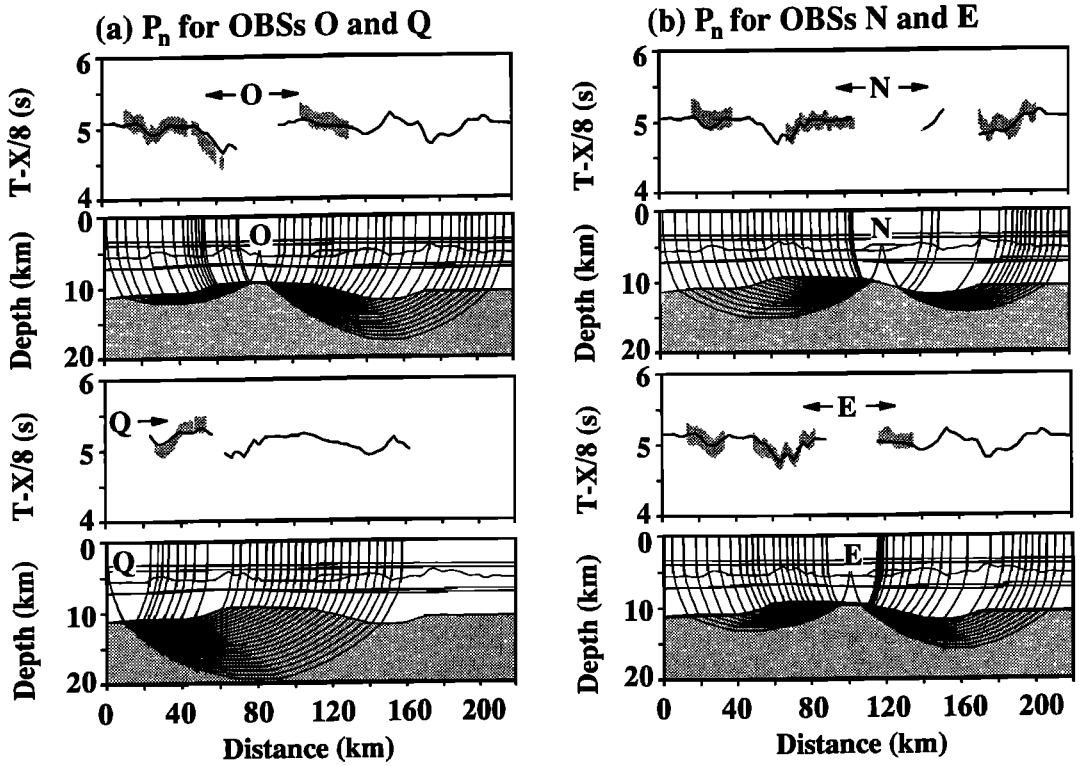

Figure 7. Computed ray paths and travel times for refractions in the mantle, P_n, using the 2-D velocity-depth structure along line R2 for (a) OBSs O and Q, (b) OBSs N and E, and (c) OBSs L and M. Observed travel times and their uncertainties are represented by the stippled areas through which the computed arrival times are traced. Ray paths converge to their corresponding receivers. For clarity, the diagrams show every other OBS for each line so that arrival times can be discriminated.

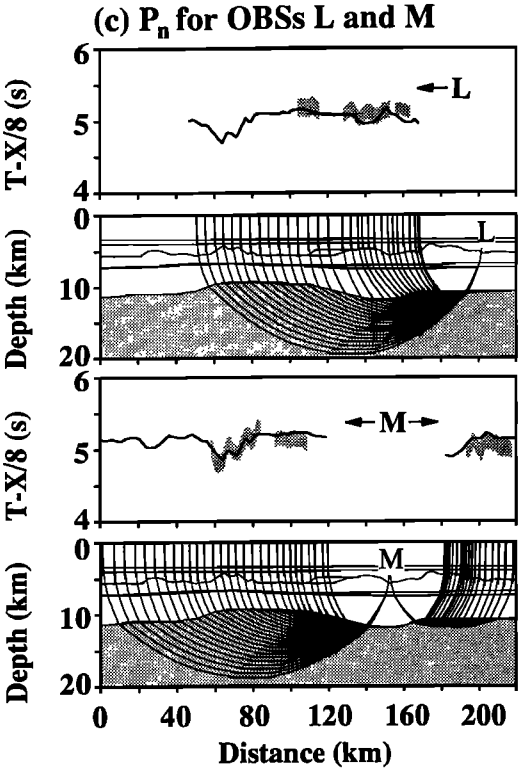

Figure 7. (continued)

extinct spreading center; and (2) the asymmetry between flanks of the extinct spreading center.

The transition from flank to extinct spreading center crustal types is marked by a combination of (1) thinning of the crust; (2) decrease in P wave velocity; and (3) a more linear velocity gradient throughout the crust. Within the extinct spreading center, arrivals at OBS O_{NE}, OBS E, and OBS N_{SW} define the upper and lower crustal structure. Low upper crustal velocities are readily apparent in Figure 6b by noting that the refractor velocities do not exceed 5 km/s. Further evidence is the marked delay in lower crustal (P_3) arrivals at OBSs E, N_{SW}, and O_{NE} (Figure 6c) which travel through the region of low upper crustal velocities within the extinct spreading center. For arrivals from the lower crust (Figure 6c), the observations of low velocities at these OBSs are even more pronounced. They are expressed in the final model by a downwarping of the 6 km/s isovelocity contour as the extinct spreading center is entered and the proximity of the 7 km/s contour to the crust-mantle boundary.

The influence of the extinct spreading center is broad, with crustal thinning observed from 50 to 120 km (Figure 5). The transition to the extinct spreading center crustal type, thin low-velocity crust with a uniform velocity gradient, occurs between 60 and 80 km on the southwest rift flank and 110 to 130 km on the northeast flank, approximately coincident with Chron 21. The crustal thickness within the paleorift valley from 80 to 110 km varies between 3.8 and 4.2 km. The thinning is defined by (1) the short shot-receiver offsets over which computed and observed refracted phases are present; and (2) the P_n arrivals, particularly the critical range at which mantle arrivals begin to be observed. The 2-D velocity-depth structure within the extinct spreading center is well constrained because receivers in this region were situated to have many overlapping ray paths in the lower crust and some in the upper crust. The four refraction profiles sampling crust in this region have $T_{RMS} \leq 0.41$ s and $\chi^2 \leq 0.49$ (Table 1, electronic supplement).

On the flanks of the extinct spreading center, 0 to 60 km to the southwest and 130 to 220 km to the northeast, the seismic behavior of the crust differs from the crust within the extinct spreading center, particularly to the northeast, with higher crustal velocities; greater ranges at which refracted arrivals are observed; 2 to 3 times more observed arrivals; and clearly discernible P_mP arrivals. The southwestern flank is defined by arrivals from OBS Q, sonobuoys 11 and 12, and OBS O_{SW}. The range from 0 to 30 km is well defined by the ray paths from OBS Q and sonobuoy 11. A typical oceanic structure is observed in this region, with a high-velocity gradient in the upper crust (isovelocity contours 4 to 6 km/s in Figure 5), a weaker velocity gradient in the lower crust (isovelocity contours 6 to 8 km/s in Figure 5), and a nominal crustal thickness of 5.5 km as defined by P_n arrivals from OBS Q, OBS O_{SW}, OBS N_{SW}, and OBS E_{SW}.

For the northeast flank, the P_3 (Figure 6c) and P_mP (Figure 6d) arrivals from OBS N_{NE}, OBS M, and OBS L_{SW} define the features of this region. The arrivals are of considerably higher velocity and extend to greater shot-receiver offsets than the arrivals at OBSs sampling the southwest flank or the extinct spreading center. To model the lower crust refractor velocities, upper boundary velocities from 6.9 to 7.2 km/s and lower boundary velocities from 7.5 to 7.7 km/s are required in the fastest region from 130 to 170 km (Table 2, electronic supplement). In addition, a thickening of the crust (by approximately 1 km) and a weak velocity gradient are required to match the shot-receiver offsets to which P_3 and P_mP arrivals are observed. From 190 to 220 km, the crustal thickness (Figure 5) is comparable to that observed on the southwest flank from 0 to 30 km, but the velocities in the lower crust are higher.

The P_mP arrivals observed on the northeast flank are used to define the velocity gradient structure of the lower crust and, in conjunction with P_n arrivals, the depth of the Moho. They are second arrivals which are difficult to pick because of interference with the wavetrain from earlier arrivals. Accordingly, they are assigned the largest travel time uncertainties of all arrivals and are intentionally the most poorly fit ($0.6 \leq \chi^2 \leq 3.8$). The final velocity-depth structure which accommodates the four sets of observed P_mP arrivals from OBS M, OBS L_{SW}, and OBS N_{NE} represents a compromise between the model revisions which individual OBSs require. For example, in the region of rapid crustal thinning from 140 to 120 km (Figure 6d), OBS M_{SW} requires a combination of slope on the crust-mantle boundary and high lower crustal velocities to reproduce the high (greater than 8 km/s) apparent move-out velocities of P_mP. The fit of computed P_mP arrivals for this OBS (χ^2=0.58) and for OBS N_{NE} (χ^2=1.78) could be improved by more rapid crustal thinning. However, the P_n arrivals from OBS N_{NE} (Figure 7b) are very sensitive to the slope of this boundary, as it controls the extent of the shadow zone encountered by rays entering the mantle. As the shadow zone broadens, the number of observed arrivals to which rays can be traced decreases.

The asymmetry between lower crustal structures observed on southwest and northeast flanks of the extinct spreading center is consistent with previous seismic and gravity observations. High-velocity lower crustal material has been observed at

widely spaced locations northeast of the extinct spreading center (Lines A and F [*Stergiopoulus*, 1984]; ODP site 646 [*Srivastava et al.*, 1989]; and line 15/77 [*Hinz et al.*, 1979]), though all but one of these refraction profiles are unreversed and may be influenced by sediment thickness variations or dipping interfaces. The presence of this material may be the cause of the regional asymmetry in the free-air gravity anomaly noted by *Srivastava et al.* [1981] north of the Minna and Cartwright Fracture Zones. It is largely positive northeast of the extinct spreading center and negative to the southwest with the degree of asymmetry increasing northwards. *Vogt et al.* [1982], in studying this regional asymmetry in the Labrador and Norwegian-Greenland Seas, find that the asymmetry is most pronounced for crust formed between magnetic anomalies 25 to 29 and weaker for the younger crust. The formation of high-velocity lower crust may be related to hot spot activity from the time of anomaly 24 until the cessation of spreading [*Srivastava et al.*, 1989], but knowledge of its regional extent will be required to address this speculation.

Mantle Layer. Ray paths and travel times for P_n (Figs. 7a, 7b and 7c) are used to define the thickness of the crust and the velocity of the uppermost mantle. These two quantities exhibit significant variations along the length of line R2, primarily in relation to distance from the extinct spreading center. In fitting the observed arrivals for P_n, T_{RMS} was kept within the uncertainty of the travel time picks (i.e., $\chi^2 \leq 1$) for seven of the 10 sets of observed arrivals (layer 8 in Table 1, electronic supplement). Model revisions were terminated when reductions in T_{RMS} for one receiver caused T_{RMS} to increase for another. For example, the largest P_n travel time residual (T_{RMS} = 0.12 s), at OBS M_{NE} (Figure 7c), may be reduced by thinning the crust or increasing the mantle velocity between 170 and 220 km. However, the arrivals for OBS L shooting southwest (Figure 7c) also travel through this region of the mantle but already arrive too early (T_{RMS}= 0.86 s). The remaining travel time residuals may be attributed to (1) limitations of 2-D methodology, with rays traveling outside the distance-depth plane assumed in the 2-D velocity-depth structure; (2) variations in the structure of an overlying layer which are not

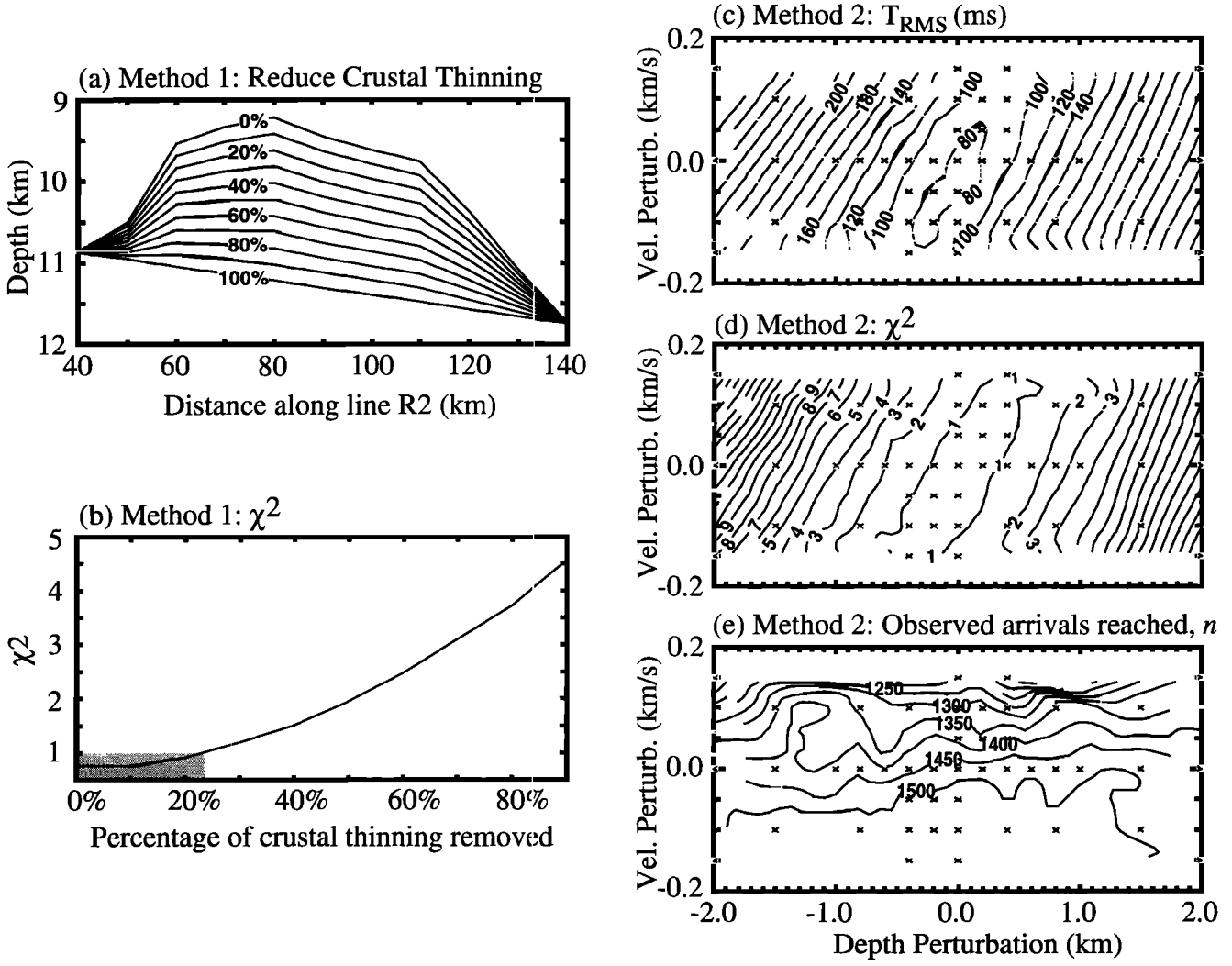

Figure 8. Error analysis along line R2. For method 1, (a) percentage is shown of crustal thinning removed within the extinct spreading center from 40 to 140 km and (b) the corresponding influence is shown on the quality of fit between observed and calculated arrival times for all mantle arrivals. For method 2, velocity and depth perturbations (stars) are introduced to nodes which form the crust-mantle boundary in the final velocity-depth structure for line R2. The effect of these perturbations on the quality of the model fit is assessed by plotting contours of (c) T_{RMS}, (d) χ^2, and (e) n.

adequately resolved by the existing data; or (3) instrument timing errors which remain at various receivers.

The isovelocity contours in Figure 5 show low velocities (< 8 km/s) in the uppermost mantle at three locations. The thickest of the low-velocity regions underlies the extinct spreading center and extends to a maximum depth of 4.3 km below the crust-mantle boundary. The upper mantle velocities within the extinct spreading center are the most well constrained in the model because of the number of overlapping ray paths and the confidence in the crustal structure overlying the mantle. The quality of the travel time fits is particularly good ($0.24 \leq \chi^2 \leq 0.58$) for the receivers which have P_n ray paths crossing or entering the mantle within the extinct spreading center (OBS E, OBS O_{NE}, OBS N_{SW}, and OBS M_{SW}). The depth of the low-velocity zone underlying the extinct spreading center complements the results obtained by 1-D WKBJ synthetic seismogram modeling for OBS G on line R1 along the axis of the extinct spreading center [*Osler and Louden*, 1992], which suggests that a relatively strong gradient exists in the uppermost mantle and extends to a depth of 3 km below the crust-mantle boundary.

Mantle arrivals help define the transition from typical oceanic crustal structures on the flanks to the distinct crustal type within the extinct spreading center, as previously mentioned. On the southwest flank, the slope on the crust-mantle boundary is revealed by the P_n arrivals at OBS O_{SW} (Figure 7a) from 45 to 60 km, which are up to 0.4 s earlier than those from 10 to 45 km. OBS Q_{NE} (Figure 7a) also defines the crust-mantle boundary on the southwest flank. For this receiver, the P_n arrivals terminate abruptly at 55 km at a shadow zone generated by the rapid crustal thinning. On the northeast flank, the transition is not as easily discerned. The high velocity lower crust in this region counteracts the delay which P_n would otherwise exhibit as the crust thickens. However, there is evidence for slope on the crust-mantle boundary from the move-out of P_mP and the shadow zone generated for P_n arrivals from OBS N shooting northeast.

Error Analysis

Error analysis of the model parameters defining the crust-mantle boundary was performed by perturbing the model parameter values and then ray tracing through the perturbed model. In the first of two approaches, the degree of crustal thinning within the extinct spreading center, as defined by boundary nodes from 40 to 140 km along line R2, was progressively decreased (Figure 8a) until the crust-mantle boundary was linear between the 40 km and 140 km endpoints. In Figure 8b, χ^2 values using the mantle arrivals at all OBSs are presented for each of these perturbed models. Following the criteria of fitting computed arrivals to within the uncertainty assigned to the observed travel time picks ($\chi^2 \leq 1$), no more than 25% of the crustal thinning may be removed before the travel time fits are no longer acceptable.

In the second approach, a constant velocity and/or depth perturbation was applied to all nodes comprising the crust-mantle boundary. Contours of T_{RMS}, χ^2, and n are presented in Figures 8c, 8d, and 8e, respectively, as a function of the velocity and depth perturbation magnitude. The T_{RMS} = 80 ms and χ^2 = 1 contours show a preferred orientation to plausible perturbations. Increases in P_n velocity are accompanied by positive depth perturbations (crustal thickening), and decreases in P_n velocity are accompanied by negative depth perturbations (crustal thinning). For positive velocity perturbations exceeding 0.05 km/s, the number of observed arrivals which are reached by the rays begins decreasing markedly (Figure 8e). The increases in the upper mantle velocities decrease the velocity gradient of the mantle layer to the point where it is too weak to refract rays to the shorter shot-receiver offsets. Using the dimensions of the 80 ms T_{RMS} contour and rejecting positive velocity perturbations, average uncertainties of ± 0.25 km and ± 0.08 km/s can be assigned to the depth and velocity nodes respectively which comprise the crust-mantle boundary.

Synthetic Seismograms

Synthetic seismograms were generated for all receivers along line R2 using TRAMP, a geometrical ray theory algorithm for inhomogeneous structures (C. Zelt, personal communication, 1992). The impulse response seismograms were convolved with a source function, the exponentially damped cosine function of *Cerveny et al.* [1977]:

$$f(t) = \exp\left[-\left(\frac{2\pi f_m}{\gamma}\right)^2 t^2\right] \cos(2\pi f_m t + \nu) \qquad (6)$$

where f_m is dominant frequency of source (6.8 Hz), γ is damping factor (5.6), ν is phase shift ($\pi/3$), and t is time. This reproduces the long wave train (approximately 450 ms) which is characteristic of the air gun source array.

A comparison of synthetic seismograms computed for a typical 1-D velocity-depth structure between TRAMP and WKBJ [*Osler*, 1993] is consistent with previous comparisons of asymptotic ray theory and its extensions (the WKBJ approximation) [e.g., *Chapman*, 1985]. These differences are most prevalent around the critical point for mantle arrivals, where asymptotic ray theory breaks down. The result is that the peak amplitude of P_mP arrivals is observed at 6 km greater range in the WKBJ synthetics and the amplitude of P_mP builds up very rapidly in the TRAMP synthetics, while it is more gradual in the WKBJ synthetics. The amplitudes of refracted arrivals compare favorably except for P_n in an interval from just beyond the critical point to a range of 40 km, where the amplitude of the TRAMP synthetics are lower than the WKBJ counterparts.

Refraction profiles at two OBS have been selected for inclusion in this paper. Observed profiles for all OBS are available on microfiche[1] (Figures A1 to A10 and B1 to B4). The synthetic seismograms and observed profiles for OBS M located northeast of the extinct spreading center are presented in Figures 9a and 9b. Shooting southwest, the high amplitude P_mP arrivals from 18 to 48 km in the observed data are matched in the synthetics from 18 to 39 km, at which point the P_mP arrivals terminate abruptly. The gap with no second arrivals and weaker first arrivals from 15 to 19 km in the observed data is also produced in the synthetics, but the interval is shifted to 17 to 21 km. The observed P_n arrivals for this receiver are particularly strong from 80 to 90 km as rays enter the southwest flank of the extinct spreading center. The

[1]Appendix figures are available with entire article on microfiche. Order from American Geophysical Union, 2000 Florida Avenue, N.W., Washington, DC 20009. Document B95-001; $2.50. Payment must accompany order.

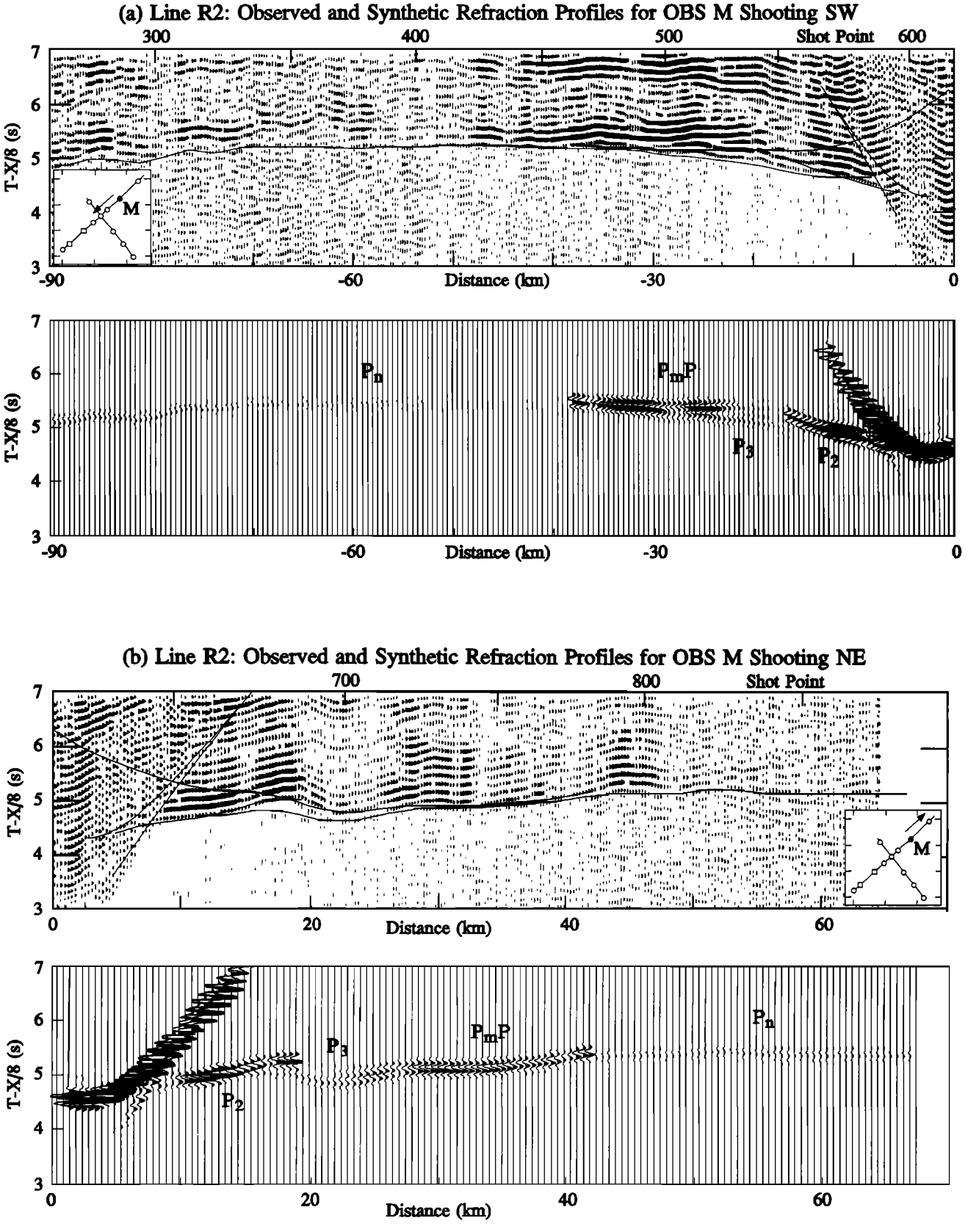

Figure 9. Observed and synthetic refraction profiles for (a) OBS M_{SW} and (b) OBS M_{NE}. Observed traces are band-pass filtered from 4 to 12 Hz; three traces are mixed. Gain is applied as a function of range, and traces are plotted at a reducing velocity of 8 km/s. Arrivals from different phases are identified on the synthetic profiles.

synthetics do not replicate this behavior. Shooting northeast, the synthetic is a particularly good representation of the data. The low amplitudes surrounding the basement high (shot point 700) are present in both the synthetics and observed data from 19 to 24 km. On either side of this feature, the synthetics match the high-amplitude arrivals from 10 to 19 km and 25 to 45 km.

The synthetic seismograms and observed profiles for OBS E located within the extinct spreading center are presented in Figures 10a and 10b. The amplitude of the upper and lower crust refracted arrivals is strong and well modeled in the synthetics, as the energy is refracted by the nearly linear velocity gradient throughout the crust within the extinct spreading center. The high amplitudes in the observed crustal arrivals are followed by strong P_n arrivals from 20 to 30 km. The synthetics put very little energy into these P_n arrivals just beyond the critical point, despite a relatively strong velocity gradient (0.04 s-1) for the upper mantle in this region.

The synthetic and observed refraction profiles compare favorably as the major amplitude variations for P_2, P_3, and P_mP arrivals are matched, although the patterns of amplitude variations are shifted by several kilometers in some instances. The greatest shortcomings of the synthetics are the low amplitude of the P_n arrivals and the very rapid termination of the P_mP arrivals. However, based on the comparison of the TRAMP and WKBJ algorithms, these shortcomings stem in part from limitations of the asymptotic ray theory which the TRAMP algorithm employs, and not solely from inadequacies in the final velocity-depth structure.

Discussion

Nature and Origin of the Crust

The seismic refraction results along the strike of the extinct spreading center [*Osler and Louden*, 1992] and crossing it transversely (this paper) find a prevalence of anomalously thin and low velocity crust in the extinct spreading center, which is underlain by low velocities in the uppermost mantle. There are two frameworks by which these observations may be explained. These consider the crust as (1) having formed through igneous extrusive and plutonic processes, then subsequently altered by tectonism; or (2) being composed of hydrothermally altered upper mantle. Oceanic crust, in the prevalent view, is igneous rock which solidifies from partial melt after it migrates to the accretionary axis. The details of this process remain equivocal, but analogies between ophiolite studies [e.g., *Salisbury and Christensen*, 1978] and marine seismic studies [e.g., *Spudich and Orcutt*, 1980] suggest that the structure of mature oceanic crust is primarily vertical, with (1) the upper crust (layer 2) composed of extrusive volcanics (pillow basalts), underlain by a dense series of vertical dikes (sheeted diabase dikes) stemming from episodes of injection from an underlying magma chamber; and (2) the lower crust (layer 3) consists of plutonically emplaced gabbros.

Assuming that the crust at the extinct spreading center formed following this general model, a pervasive fracturing of the entire crust is a mechanism for thinning the crust and lowering its velocity. In this scenario, decreases in spreading rate preceding extinction would be associated with a decrease in magmatism and an increasing requirement for tectonism to accommodate the divergence of the plates. This association is supported by a number of studies. *Huang and Solomon* [1988] present observations that the maximum centroid depth of active ridge crest earthquakes increases from 2-3 km at full spreading rates of 40-45 mm/yr to 5-6 km at full spreading rates of 5-10 mm/yr. *Purdy et al.* [1992] show that a systematic relationship exists between spreading rate and the depth to which a P wave velocity inversion is observed at active spreading centers. Their preferred explanation is that the "major faults that extend to greater depths on slower-spreading ridges [*Huang and Solomon*, 1988] and allow a more vigorous circulation of cooling sea water to reach greater depths, blocking the upward migration of large melt bodies" [*Purdy et al.*, 1992]. The maximum depth to which faulting extends is an indication of the thickness of the mechanically strong layer which is prone to brittle failure in response to the extensional stresses caused by the diverging plates. Through an examination of the throw on normal faults at slow spreading centers, *Macdonald and Luyendyk* [1977] suggest that up to 20% of the plate divergence may be accommodated by these faults. Last, there are compilations of seismic refraction data which document that crustal thickness becomes a function of spreading rate when the spreading rate is less than 15 mm/yr [*Reid and Jackson*, 1981; *Bown and White*, 1994].

A systematic relationship between spreading rate, faulting, hydrothermal circulation, and the depth below the spreading center at which an appreciable partial melt fraction is observed could be readily applied to the spreading center in the Labrador Sea preceding its extinction. The zone in which crustal and upper mantle velocities are anomalously low and the crustal thinning occurs is bounded within anomalies 21 west and 21 east (Figures 1 and 5) where the slowest spreading rates are encountered. It is within this region that the crust should be most susceptible to brittle failure, thinning by tectonism, and a reduced partial melt supply due to conductive cooling of melt bodies. This hypothesis is supported by a multichannel seismic reflection profile crossing the extinct spreading center to the south of line R2. *Srivastava et al.* [1993] find evidence for crustal extension by rotated crustal blocks between anomalies 21 west and 21 east.

A second view of the anomalous crustal structure within the extinct spreading center is one in which it is formed by the serpentinization of upper mantle peridotite [*Hess*, 1962; *Lewis and Snydsman*, 1979]. The Moho in this case would not represent a compositional change between crust and mantle but the depth to which upper mantle was hydrothermally altered. The crustal P wave velocities observed would be a linear function of the volume percentage of serpentinite, velocities of approximately 5 km/s for 100% serpentinite increasing to 8.0 km/s for unaltered peridotite [*Christensen*, 1966]. Serpentinite has a V_p/V_s ratio which is much higher than other rocks likely to constitute the oceanic crust. It is on the basis of V_p/V_s studies [*Christensen*, 1972] that the serpentinite model of normal oceanic crust has been largely rejected. However, it remains a viable alternative for the structure of the crust at oceanic fracture zones [*Calvert and Potts*, 1985; *Louden et al.*, 1986] and has been applied as an alternative model for the East Pacific Rise based on gravity data and thermal models [*Lewis*, 1983].

In the serpentinite model, the variable thickness of the crust along the strike of the extinct spreading center, the linear velocity gradients and the low crustal velocities (line R1, 1-D travel time solutions and τ-p inversions [*Osler and*

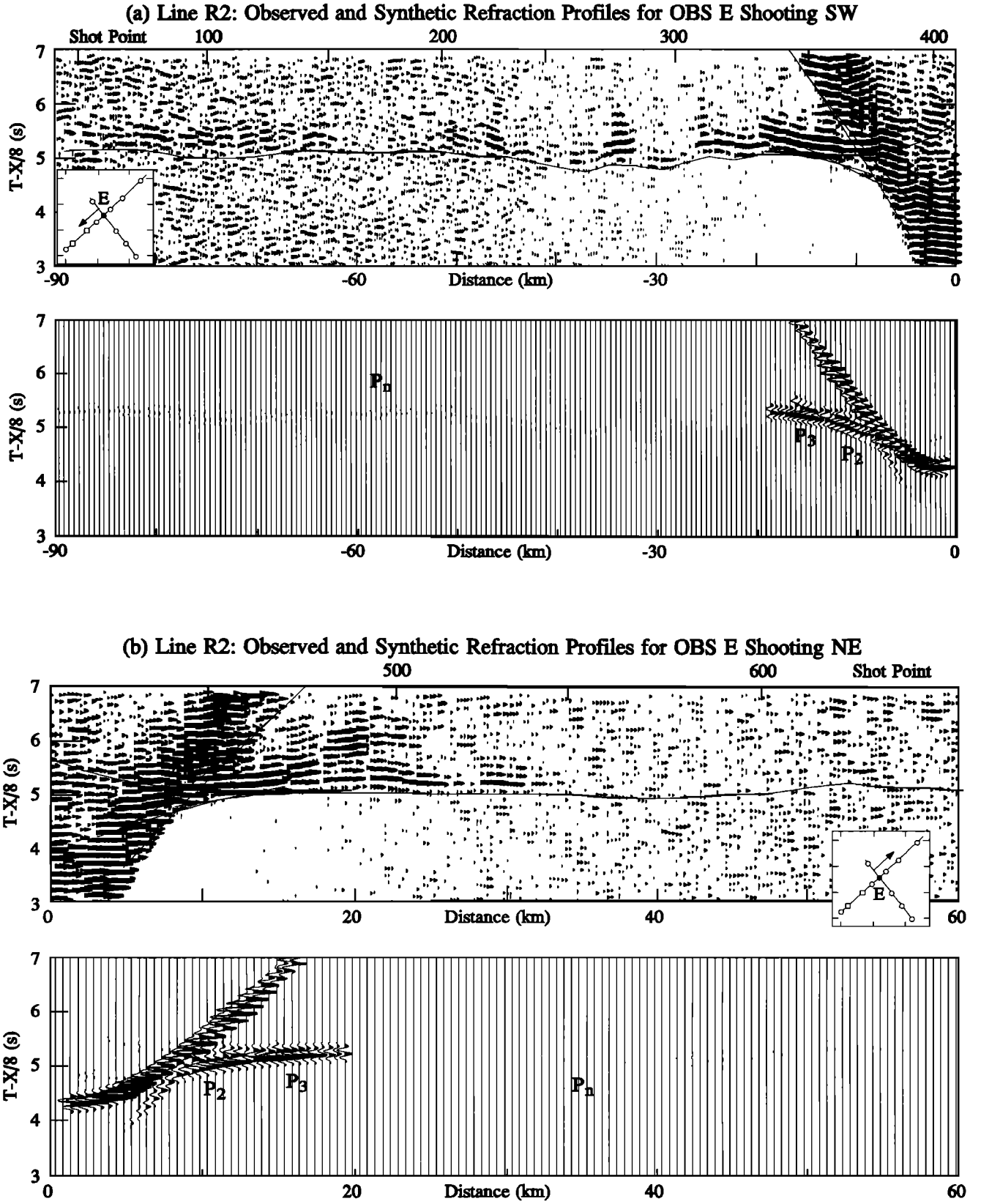

Figure 10. Observed and synthetic refraction profiles for (a) OBS E_{SW} and (b) OBS E_{NE}. Observed traces are band-pass filtered from 4 to 12 Hz; three traces are mixed. Gain is applied as a function of range and traces are plotted at a reducing velocity of 8 km/s. Arrivals from different phases are identified on the synthetic profiles.

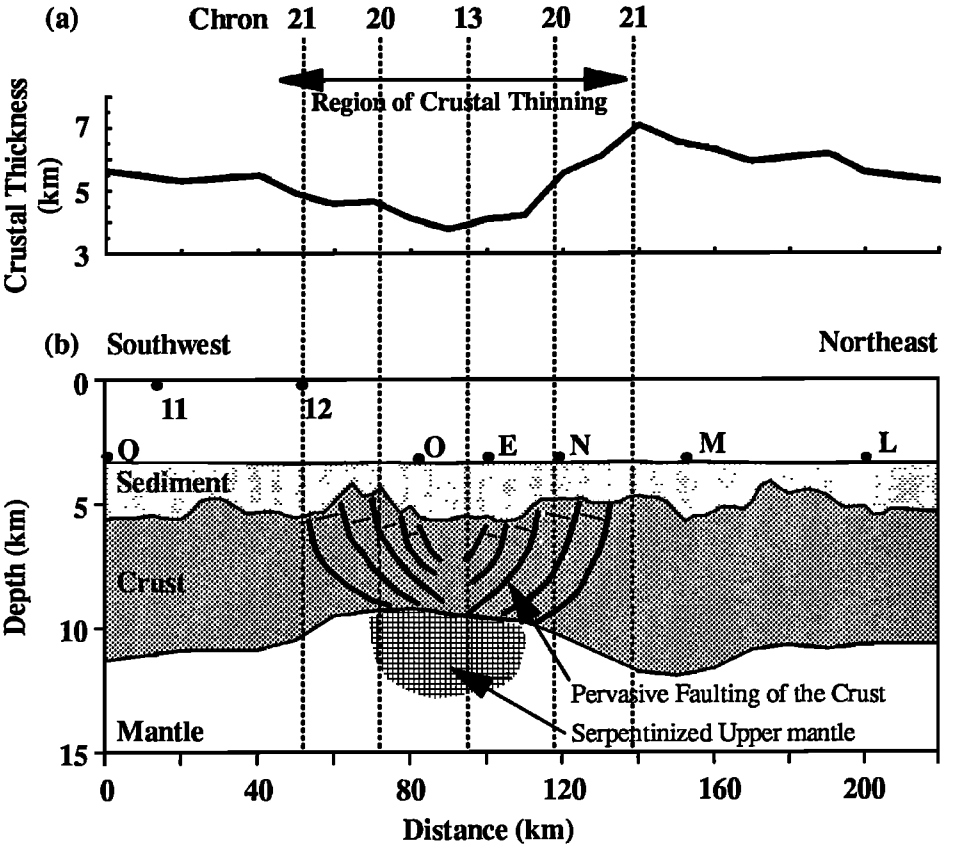

Figure 11. Summary of results along line R2 transversely crossing the extinct spreading center in the Labrador Sea. (a) Crustal thickness at each mantle boundary node in the 2-D seismic modeling and (b) the suggested relationship between the crustal thinning, low crustal P wave velocities and hydrothermal alteration of the upper mantle due to faulting and reduced partial melt supply at the slow spreading rates preceding the extinction of the spreading center.

Louden, 1992]) may be explained in terms of the regional variability in the depth to which hydrothermal circulation has penetrated and altered the upper mantle. However, the presence of velocity gradients in the upper mantle beneath the Moho requires a further complexity. Two stages of hydrothermal alteration would need to have been operative: one that is quite vigorous and short lived to establish the distinct boundary interpreted as the Moho and a second that is more protracted to alter rocks below this boundary. While this mechanism is largely speculative, multiple stages of hydrothermal alteration are required to explain the petrology of gabbroic rocks dredged from the failed Mathematician Ridge in the eastern Pacific Ocean [*Stakes and Vanko*, 1986]. An initial high-temperature vapor phase is purported to be followed by a more pervasive lower-temperature brine phase.

A crustal layer which is discrete from the mantle is more easily explained by the igneous model in which the velocity of the crust is lowered by pervasive fracturing and thinned by increased tectonism and decreased partial melt supply. The faults provide a pathway for fluids to penetrate into the uppermost mantle and alter the peridotite (Figure 11). A preexisting Moho is thus overprinted by one episode of hydrothermal alteration. Discrimination between these alternatives would require V_p/V_s ratios for the crustal level material. S-waves are observed on some OBSs; however, they are not well developed and only show arrivals for the mantle refraction, S_n.

Nature and Origin of the Upper Mantle

Low velocities are observed in the upper mantle in four of the seven refraction profiles shot on line R1 along the strike of the extinct spreading center [*Osler and Louden*, 1992]. The average upper mantle velocity is 7.74 km/s, which is less than the velocities of 7.92, 7.82, and 7.94 km/s determined for the three upper mantle nodes within the extinct spreading center in this study (Table 2, electronic supplement). This difference in velocity may be attributed to azimuthal anisotropy in the mantle [*MacKenzie*, 1972; *Bibee and Shor*, 1976].

The low velocities are interpreted as resulting from the hydrothermal alteration of upper mantle peridotite. The pathway for hydrothermal alteration of the upper mantle (Figure 11) could be provided by faults extending through the crust. No more than 10% of the peridotite must be serpentinized to produce the observed velocities [*Christensen*, 1966]. There is evidence for hydrothermal alteration and serpentinization at oceanic fracture zones [e.g., *Calvert and Potts*, 1985; *Christensen*, 1972; *Minshull et al.*, 1991]. Hydrothermal alteration is called upon by *Calvert and Potts* [1985] to explain the widespread occurrence of low upper mantle velocities in old Atlantic fracture zones and an apparent decrease in upper mantle velocity in fracture zones with increasing age. Given the similarity between the crustal structures observed within the extinct spreading center to those at oceanic fracture zones [*Osler and Louden*, 1992] and

the likelihood of faults penetrating the entire crust at the slow spreading rates preceding extinction, the extinct spreading center is an environment in which upper mantle peridotite are liable to be serpentinized.

Comparison to Crustal Processes at Active Slow Spreading Centers

At the Mid-Atlantic Ridge, recent studies suggest that within a ridge segment there is considerable along-axis variation in the thermal and mechanical properties of the lithosphere. The studies include along axis seismic refraction [*Purdy and Detrick*, 1986], high-resolution multibeam bathymetry mapping [*Sempere et al.*, 1990], multichannel seismic reflection [*Detrick et al.*, 1990], 3-D gravity studies [*Kuo and Forsyth*, 1988; *Lin et al.*, 1990], microearthquake source locations and delay time tomography [*Toomey et al.*, 1988; *Kong et al.* 1992], and geochemical studies [*White et al.*, 1992].

An important consensus emerging from these studies at slow spreading centers is that crustal accretion is an episodic and not a steady state process and crustal accretion must be focused at the center of the ridge segment [*Ballard and Francheteau*, 1983; *Solomon and Toomey*, 1992; *White et al.*, 1984]. As there is no seismic evidence supporting the presence of steady state axial magma chambers at slow spreading centers [*Detrick et al.*, 1990], magmatism at the crustal level is considered to be an intermittent process. Consequently, plate divergence at slow spreading centers is partially accommodated through lithospheric stretching [*Macdonald and Luyendyk*, 1977]. Along-axis, ridge segment ends appear to experiencing more tectonism than the axial high where crustal accretion is focused [*Huang and Solomon*, 1988; *Lin and Bergman*, 1990]. The ends of the ridge segments are cooler than any other portion of the ridge segment because of their proximity to the cold lithosphere against which they are juxtaposed. Consequently, they are mechanically stronger are more prone to brittle failure than other portions of the ridge crest. The ends of ridge segments are also areas where the production of partial melt supply and/or its transport is most severely limited [*Phipps Morgan and Forsyth*, 1988].

The processes which occur during the extinction of a spreading center have an analog in the spatial relationship between the center of a ridge axis and its fracture zones. The parallels are (1) the presence of brittle crust due to thermal regime, hot and cold lithosphere juxtaposed at a fracture zone and a dissipating thermal anomaly at a dying spreading center; (2) the effects of tectonism which thin the brittle crust directly through crustal extension accommodated by rotated crustal blocks or indirectly by reducing partial melt supply; and (3) the provision of a pathway for hydrothermal alteration of the upper mantle. At the extinct spreading center, the decreases in spreading rate which precede the extinction of a spreading center enhance cooling of the crust by conduction. This leads to an increase in tectonism as the crust becomes brittle. The increased tectonism promotes deeper penetration of conductive cooling which restricts partial melt supply. Serpentinization of the upper mantle ensues once the crust has been faulted and deep hydrothermal circulation occurs.

Conclusion

A 2-D seismic velocity-depth structure (Figure 5) was developed for refraction line R2 transversely crossing the extinct spreading center in the Labrador Sea. Information from 12 kHz bathymetry data, seismic reflection data, and plane layer and τ-p 1-D travel time solutions were used to develop an initial velocity-depth structure. The final velocity-depth structure was obtained by revising this initial velocity-depth structure to improve (1) the fit between arrival times calculated by ray tracing and their observed counterparts; and (2) the fit between amplitude patterns in synthetic and observed refraction profiles.

Crust within the extinct spreading center is found to be thin and of anomalously low P wave velocity when compared with mature oceanic crust. It is underlain by low upper mantle velocities which may exhibit some anisotropy. The low crustal velocities are attributed to an increase in the degree of tectonism preceding extinction, which pervasively fractured the crust (Figure 11). This faulting also provides a pathway for hydrothermal alteration of the upper mantle peridotite and is the manner by which the low velocities in the uppermost mantle are produced. The lateral extent of the thinning and occurrence of low-velocity crust are coincident with the time interval in which spreading rate in the Labrador Sea decreased most rapidly (Chron 21 until the cessation of spreading). This observation supports a systematic relationship between spreading rate, faulting, hydrothermal circulation, and partial melt supply at active spreading centers. A subsequent paper will extend the seismic results presented in this paper by considering gravity models which are based on the proposed seismic velocity-depth structure and plausible spreading rate histories for the Labrador Sea based on modeling of magnetic anomalies.

Acknowledgments. We would like to thank the officers and crew of the C.S.S. *Hudson*, Borden Chapman, Guy Fehn, and Neil Hamilton, for their technical expertise during the course of the seismic refraction experiment. The analog refraction data were replayed and digitized using computing facilities at the Bedford Institute of Oceanography with the assistance of Steve Peary and Ian Reid. The development of processing algorithms for the refraction data was assisted in its infancy by Greg Leger and the staff of the Dalhousie University Computing and Information Services and more recently by Deping Chian and Saeid Yazdanmehr. The research was supported by Energy, Mines and Resources grant 30/04/87 and Natural Science and Engineering Research Council of Canada grants OGP0008459, EQP0027418, and INF0001469. J.C.O. acknowledges financial support provided by a fellowship from Dalhousie University. Comments on the original manuscript by J. Austin, D. Hutchinson, and an anonymous reviewer are greatly appreciated.

References

Anderson, R.N., and J.G. Sclater, Topography and evolution of the East Pacific Rise between 5°S and 20°S, *Earth Planet. Sci. Lett.*, *14*, 433-441, 1972.

Ballard, R. D., and J. Francheteau, Geologic processes of the mid-ocean ridge and their relation to sulfide deposition, in *Hydrothermal Processes at Seafloor Spreading Centers*, edited by P. A. Rona et al., pp. 141-168, Plenum, New York, 1983.

Batiza, R., Failed rifts, in *The Geology of North America*, vol. N, *The Eastern Pacific Ocean and Hawaii*, edited by E. L. Winterer, D. M. Hussong, and R. Decker, pp. 177-186, Geological Society of America, Boulder, Colo., 1989.

Bibee, L. D., and G. G. J. Shor, Compressional wave anisotropy in the crust and upper mantle, *Geophys. Res. Lett.*, *3*, 639-642, 1976.

Bown, J. W., and R. S. White, Variation with spreading rate of oceanic crustal thickness and geochemistry, *Earth Planet. Sci. Lett.*, 121, 435-449, 1994.

Calvert, A. J., and C. G. Potts, Seismic evidence for hydrothermally

altered mantle beneath the old crust of the Tydeman fracture zone, *Earth Planet. Sci. Lett.*, *75*, 439-449, 1985.

Cerveny, V., I. Molotkov, and I. Psencik, *Ray Method in Seismology*, University of Karlova, Prague, Czechoslovakia, 1977.

Chapman, C. H., 1985, Ray theory and its extensions: WKBJ and Maslov seismograms, *J. Geophys.*, *58*, 27-43, 1985.

Christensen, N. I., Elasticity of ultrabasic rocks, *J. Geophys. Res.*, *71*, 5921-5931, 1966.

Christensen, N. I., The abundance of serpentinites in the oceanic crust, *J. Geol.*, *80*, 709-719, 1972.

Denham, C. R., and H. Schouten, On the likelihood of mixed polarity in oceanic basement drill cores, in *Implications of Deep Drilling Results in the Atlantic Ocean: Ocean Crust, Maurice Ewing Ser.*, vol. 2, edited by M. Talwani et al., pp. 160-165, AGU, Washington, D.C., 1979.

Detrick, R. S., J. C. Mutter, P. Buhl, and I. Kim, No evidence from multichannel reflection data for a crustal magma chamber in the MARK area on the Mid-Atlantic Ridge, *Nature*, *347*, 61-64, 1990.

Drake, C. L., N. J. Campbell, G. Sander, and J. E. Nafe, A mid-Labrador Sea ridge, *Nature*, *200*, 1085-1086, 1963.

Hess, H. H., History of ocean basins, in *Petrologic Studies: Buddington Volume*, pp. 599-620, Geological Society of America, Boulder, Colo., 1962.

Hinz, K., H. U. Schlüter, A. C. Grant, S. P. Srivastava, D. Umpleby, and J. Woodside, Geophysical transects of the Labrador Sea: Labrador to southwest Greenland, *Tectonophysics*, *59*, 151-183, 1979.

Huang, P. Y., and S. C. Solomon, Centroid depths of mid-ocean ridge earthquakes: Dependence on spreading rate, *J. Geophys. Res.*, *93*, 13,445-13,477, 1988.

Hyndman, R. D., Evolution of the Labrador Sea, *Can. J. Earth Sci.*, *10*, 637-644, 1973.

Jarrard, R. D., K. A. Dadey, and W. H. Busch, Velocity and density of sediments in the Eirik Ridge, Labrador Sea: Control by porosity and mineralogy, *Proc. Ocean Drill. Program, Sci. Results*, *105*, 811-835, 1989.

Kent, D.V., and F. M. Gradstein, A Jurassic to recent chronology, in *The Geology of North America*, vol. M, *The Western North Atlantic Region*, edited by P.R. Vogt and B. E. Tucholke, pp. 45-50, Geological Society of America, Boulder, Colo., 1986.

Klitgord, K. D., and J. Mammerickx, Northern East Pacific Rise: Magnetic anomaly and bathymetric framework, *J. Geophys. Res.*, *87*, 6725-6750, 1982.

Kong, L. S. L., S. C. Solomon, and G. M. Purdy, Microearthquake characteristics of a mid-ocean ridge along-axis high, *J. Geophys. Res.*, *97*, 1659-1686, 1992.

Kristoffersen, Y., and M. Talwani, Extinct triple junction south of Greenland and the Tertiary motion of Greenland relative to North America, *Geol. Soc. Am. Bull.*, *88*, 1037-1049, 1977.

Kuo, B., and D. Forsyth, Gravity anomalies of the ridge-transform system in the South Atlantic between 31 and 34.5°S: Upwelling centers and variations in crustal thickness, *Mar. Geophys. Res.*, *10*, 205-232, 1988.

Lewis, B. T. R., The East Pacific Rise and the thermal model, *J. Geophys. Res.*, *88*, 3348-3354, 1983.

Lewis, S. D., and D. E. Hayes, The structure and evolution of the Central Basin Fault, West Philippine Basin, in *The Tectonic and Geologic Evolution of Southeast Asian Seas and Islands, Geophys. Monogr. Ser.*, vol. 23, pp. 77-88, AGU, Washington, D.C., 1980.

Lewis, B. T. R., and W. E. Snydsman, Fine structure of the lower crust on the Cocos Plate, *Tectonophysics*, *55*, 87-105, 1979.

Lin, J., and E. A. Bergman, Rift grabens, seismicity, and volcanic segmentation of the Mid-Atlantic Ridge: Kane to Atlantis fracture zones (abstract), *Eos Trans. AGU*, *71*, 1572, 1990.

Lin, J., G. M. Purdy, H. Schouten, J. C. Sempere, and C. Zervas, Evidence from gravity data for focused magmatic accretion along the Mid-Atlantic Ridge, *Nature*, *344*, 627-632, 1990.

Loncarevic, B. D., Ocean bottom seismometry, in *CRC Handbook of Geophyscial Exploration at Sea*, edited by R.A. Geyer, pp. 219-263, CRC Press, Boca Raton, Fla., 1983.

Louden, K. E., R. S. White, C. G. Potts, and D. W. Forsyth, Structure and seismotectonics of the Vema fracture zone, Atlantic Ocean, *J. Geol. Soc. London*, *143*, 795-805, 1986.

Macdonald, K. C., and B. P. Luyendyk, Deep-tow studies of the structure of the Mid-Atlantic Ridge crest near lat 37°N, *Geol. Soc. Am. Bull.*, *88*, 621-636, 1977.

MacKenzie, D. B., Peridotite fabrics and velocity anisotropy in the Earth's mantle, *Mem. Geol. Soc. Am.*, *132*, 593-603, 1972.

Mammerickx, J., and D. Sandwell, Rifting of old oceanic lithosphere, *J. Geophys. Res.*, *91*, 1975-1988, 1986.

Minshull, T. A., R. S. White, J. C. Mutter, P. Buhl, R. S. Detrick, C. A. Williams, and E. Morris, Crustal structure at the Blake Spur Fracture Zone from expanding spread profiles, *J. Geophys. Res.*, *96*, 9955-9984, 1991.

Nagumo, S., T. Ouchi, and S. Koresawa, Seismic velocity structure near the extinct spreading center in the Shikoku Basin, North Philippine Sea, *Mar. Geol.*, *35*, 135-146, 1980.

Osler, J. C., Crustal structure of the extinct spreading center in the Labrador Sea: Implications for dynamic models of flow beneath mid-ocean ridges, Ph.D. thesis, Dalhousie Univ., Halifax, Nova Scotia, 1993.

Osler, J. C., and K. E. Louden, Crustal structure of an extinct rift axis in the Labrador Sea: Preliminary results from a seismic refraction survey, *Earth Planet. Sci. Lett.*, *108*, 243-258, 1992.

Phipps Morgan, J., and D. Forsyth, Three-dimensional flow and temperature perturbations due to a transform offset: Effects on oceanic crustal and upper mantle structure, *J. Geophys. Res.*, *93*, 2955-2966, 1988.

Purdy, G. M., and R. S. Detrick, Crustal structure of the Mid-Atlantic Ridge at 23°N from seismic refraction studies, *J. Geophys. Res.*, *91*, 3739-3762, 1986.

Purdy, G. M., L. S. L. Kong, G. L. Christeson, and S. C. Solomon, Relationship between spreading rate and the seismic structure of mid-ocean ridges, *Nature*, *355*, 815-817, 1992.

Reid, I., and H. R. Jackson, Ocean spreading rate and crustal thickness, *Mar. Geophys. Res.*, *5*, 165-172, 1981.

Roest, W. R., and S. P. Srivastava, Sea-floor spreading in the Labrador Sea: A new reconstruction, *Geology*, *17*, 1000-1003, 1989a.

Roest, W. R., and S. P. Srivastava, Seafloor spreading history, I, Magnetic anomalies along track, in *East Coast Basin Atlas Series: Labrador Sea*, coordinated by J.S. Bell, p. 98, Geological Survey of Canada, Atlantic Geoscience Centre, Dartmouth, Nova Scotia, 1989b.

Roots, W. D., and S. P. Srivastava, Origin of marine magnetic quiet zones in the Labrador and Greenland Seas, *Mar. Geophys. Res.*, *6*, 395-408, 1984.

Salisbury, M. H., and N. I. Christensen, The seismic velocity structure of a traverse through the Bay of Islands ophiolite complex, Newfoundland, an exposure of oceanic crust and upper mantle, *J. Geophys. Res.*, *83*, 805-817, 1978.

Sempere, J., G. M. Purdy, and H. Schouten, Segmentation of the Mid-Atlantic Ridge between 24°N and 30°40'N, *Nature*, *344*, 427-431, 1990.

Solomon, S. C., and D. R. Toomey, The structure of mid-ocean ridges, *Annu. Rev. Earth Planet. Sci.*, *20*, 329-364, 1992.

Spudich, P., and J. Orcutt, A new look at the seismic velocity structure of the oceanic crust, *Rev. Geophys.*, *18*, 627-645, 1980.

Srivastava, S. P., Evolution of the Labrador Sea and its bearing on the early evolution of the North Atlantic, *Geophys. J. R. Astron. Soc.*, *52*, 313-357, 1978.

Srivastava, S. P., R. K. H. Falconer, and B. MacLean, Labrador Sea, Davis Strait, Baffin Bay: geology and geophysics-A review, *Mem. Can. Soc. Pet. Geol.*, *7*, 333-398, 1981.

Srivastava, S. P., C. G. Powell, A. G. Nunns, L. C. Kovacs, D. G. Roberts, M. T. Jones, C. Uruski, and D. Voppel, Magnetic anomalies of total intensity, in *Geophysical Atlas of the North Atlantic Between 50° to 70°N and 0° to 65°W*, edited by S. P. Srivastava, D. Voppel, and B. Tucholke, pp. 3-4, Deutsches Hydrographisches Institut, Hamburg, 1988.

Srivastava, S. P., K. E. Louden, S. Chough, D. Mosher, B. D. Loncarevic, P. Mudie, A. de Vernal, and B. MacLean, Results of

detailed geological and geophysical measurements at ODP sites 645 in Baffin Bay and 646 and 647 in the Labrador Sea, *Proc. Ocean Drill. Program, Sci. Results, 105*, 891-922, 1989.

Srivastava, S. P., C.E. Keen, and P. Potter, Crustal extension in the Labrador Sea: Evidence from multichannel seismic reflection data (abstract), *Eos Trans. AGU, 74,* Fall Meeting suppl., 605, 1993.

Stakes, D., and D. A. Vanko, Multistage hydrothermal alteration of gabbroic rocks from the failed Mathematician Ridge, *Earth Planet. Sci. Lett., 79*, 75-92, 1986.

Stergiopoulus, A. B., Geophysical crustal studies off the SW Greenland margin, M. Sc. thesis, Dalhousie Univ., Halifax, Nova Scotia, 1984.

Talwani, M., and O. Eldholm, Evolution of the Norwegian-Greenland Sea, *Geol. Soc. Am. Bull, 88*, 969-999, 1977.

Tomoda, Y., K. Kobayashi, J. Segawa, M. Nomura, and K. Kimura, Linear magnetic anomalies in the Shikoku Basin, northeastern Philippine Sea, *J. Geomagn. Geoelectr., 28*, 47-56, 1975.

Toomey, D. R., S. C. Solomon, and G. M. Purdy, Microearthquakes beneath the median valley of the Mid-Atlantic Ridge near 23°N: Tomography and tectonics, *J. Geophys. Res., 93*, 9093-9112, 1988.

Van der Linden, W. J., Crustal attenuation and seafloor spreading in the Labrador Sea, *Earth Planet. Sci. Lett., 27*, 409-423, 1975.

Vogt, P. R., L. C. Kovacs, C. Bemero, and S. P. Srivastava, Asymmetric geophysical signatures in the Greenland-Norwegian and southern Labrador Seas and the Eurasia basin, *Tectonophysics, 89*, 95-160, 1982.

Weissel, J. K., and D. E. Hays, Evolution of the Tasman Sea reappraised, *Earth Planet. Sci. Lett., 36*, 77-84, 1977.

Weissel, J. K., and A. B. Watts, Tectonic evolution of the Coral Sea Basin, *J. Geophys. Res., 84*, 4572-4582, 1979.

White, R. S., R. S. Detrick, M. C. Sinha, and M. H. Cormier, Anomalous seismic crustal structure of oceanic fracture zones, *Geophys. J. R. Astron. Soc., 79*, 779-798, 1984.

White, R. S., D. P. McKenzie, and R. K. O'Nions, Ocean crustal thickness from seismic measurements and rare earth element inversions, *J. Geophys. Res., 97*, 19,683-19,716, 1992.

Woodside, J., Geophysics II, Gravity anomaly, in *East Coast Basin Atlas Series: Labrador Sea*, coordinated by J.S. Bell, p. 94, Geological Survey of Canada, Atlantic Geoscience Centre, Dartmouth, Nova Scotia, 1989.

Zelt, C. A., and R. B. Smith, Seismic traveltime inversion for 2-D crustal velocity structure, *Geophys. J. Int., 108*, 16-34, 1992.

K. E. Louden, Department of Oceanography, Dalhousie University, Halifax, Nova Scotia, Canada B3H 4J1. (e-mail: keith@papa.ocean.dal.ca).

J. C. Osler, Defence Research Establishment Atlantic, Dartmouth, Nova Scotia, Canada B2Y 3Z7. (e-mail: osler@maggie.drea.dnd.ca)

(Received February 21, 1994; revised October 31, 1994; accepted November 2, 1994.)